Available online at www.sciencedirect.com
SCIENCE DIRECT®

International Journal of Heat and Mass Transfer 48 (2005) 585–598

International Journal of HEAT and MASS TRANSFER

www.elsevier.com/locate/ijhmt

Experiments for liquid phase mass transfer rate in annular regime for a small vertical tube

Tomio Okawa *, Akio Kotani, Isao Kataoka

Department of Mechanophysics Engineering, Osaka University, 2-1, Yamadaoka, Suita-shi, Osaka 565-0871, Japan

Received 13 February 2004; received in revised form 13 August 2004
Available online 5 November 2004

Abstract

The double film extraction technique was used to measure the deposition rate and the entrainment rate of droplets for vertical upward annular two-phase flow in a small diameter tube. The test section was a round tube of 5 mm in inside diameter, air and water were used as test fluids and the system pressure was varied within 0.14–0.76 MPa. It was shown in the present experimental conditions that the deposition rate was primarily influenced by the droplet concentration in the gas core and that the entrainment rate was correlated well with the dimensionless number denoting the ratio of interfacial shear force to surface tension force acting on the surface of liquid film. These results were consistent with available empirical correlations that were developed using the experimental data for larger diameter tubes.

Keywords: Annular flow; Mass transfer rate; Deposition; Entrainment; Small tube; Experiment

1. Introduction

Annular flow is a particularly important flow pattern in gas–liquid two-phase flow since it occurs in a wide range of vapor quality. In this flow pattern, the liquid phase moves partly as a liquid film on the tube wall and partly as droplets in the vapor core. There exists mass transfer between the liquid film and droplets because of the deposition of droplets and the atomization of liquid film. It is known that, to a good approximation, the occurrence of critical heat flux condition in annular regime corresponds to the disappearance of liquid film [1]. Using this knowledge, the film flow analysis that is one of the most successful methods to predict the onset of critical heat flux condition in annular regime was developed [2]. The basic equation used in the film flow analysis is given by

$$\frac{dG_f}{dz} = \frac{4}{D}(m_d - m_e - m_v) \tag{1}$$

where z is the distance along the flow channel, G_f is the mass flux of liquid film, D is the tube diameter; m_d, m_e and m_v are the deposition rate, entrainment rate and vaporization rate per unit area of the tube wall, respectively. If Eq. (1) is integrated from the starting point of annular flow to the exit of heated channel, G_f is given as a function of z. The heat flux that is applied when the local film flowrate becomes sufficiently small is considered as the critical heat flux. It is recognized from Eq. (1) that the valid constitutive relations for m_d and m_e are indispensable in the prediction of critical heat flux with this method.

* Corresponding author. Tel.: +81 6 6879 7257; fax: +81 6 6879 7247.
E-mail address: t-okawa@mech.eng.osaka-u.ac.jp (T. Okawa).

0017-9310/$ - see front matter © 2004 Elsevier Ltd. All rights reserved.
doi:10.1016/j.ijheatmasstransfer.2004.08.030

Nomenclature

C	droplet concentration in gas core (kg/m^3)
D	tube diameter (m)
E	entrainment fraction
F	correction function for z^*
f	friction factor
G	mass flux (kg/m^2 s)
g	gravitational acceleration (m/s^2)
J	volumetric flux (m/s)
J^*	dimensionless volumetric flux
k_d	deposition mass transfer coefficient (m/s)
k_{d0}	k_d when z_d approaches zero (m/s)
k_e	proportionality factor for m_e (m/s)
m_d	deposition rate (kg/m^2 s)
m_e	entrainment rate (kg/m^2 s)
m_v	vaporization rate (kg/m^2 s)
P	pressure (Pa)
Pr	Prandtl number
Re	Reynolds number
We	Weber number
z	distance along the channel (m)
z_d	deposition length (m)
z^*	dimensionless deposition length

Greek symbols

δ	film thickness (m)
μ	viscosity (Pa s)
π_e	ratio of interfacial shear force to surface tension force
ρ	density (kg/m^3)
σ	surface tension (N/m)

Subscripts

1	first film extraction unit
2	second film extraction unit
c	critical
d	droplet
eq	equilibrium
f	liquid film
g	gas phase
i	interfacial
k	g or l
l	liquid phase
w	wall

A number of experimental measurements for m_d have been reported in literature [3–8]. Several techniques including the film removal and redeposition (double film extraction) method [3–5], the thermal (heat balance) method [6] and the tracer mixing method [7,8] were adopted in the measurements. The principles of these measurement techniques are described by Hewitt [9]. Bennett et al. [10] showed that m_d can also be deduced from the critical heat flux data for the tube with axially non-uniform heating [10–16] if the position for the occurrence of burnout can be specified. The important characteristics of these experiments for m_d are presented in Tables 1 and 2.

In adiabatic experiments, annular flow reaches quasi-equilibrium state sufficiently downstream from the gas–liquid mixing section. In the equilibrium state, the flowrates of liquid film and droplets are almost constant along the channel since m_d is balanced with m_e. Hence, the experimental data for m_d measured in the quasi-equilibrium state is expected the good approximation for m_e [5]. It is also possible to deduce m_e from the experimental data of equilibrium entrainment fraction E_{eq} [17]. In order to express m_d with simple equations, it is generally assumed that m_d is proportional to the droplet concentration in the gas core C through a deposition mass transfer coefficient k_d

$$m_d = k_d C \tag{2}$$

Postulating that the liquid film is thin and the relative velocity between the gas phase and droplets is small, the following relation for equilibrium annular flow is obtained from Eq. (2):

$$m_e \cong m_d = k_d C \cong k_d \frac{\rho_g E_{eq} G_l}{G_g} \tag{3}$$

where ρ_g is the gas density; G_g and G_l are the mass fluxes of gas and liquid phases, respectively. Eq. (3) implies that m_e is calculated from E_{eq} if a reliable correlation for k_d is available. The experiments for E_{eq} available in literature are summarized in Table 3 [3,8,18–27].

Tables 1–3 indicate that the measurements for m_d and m_e were conducted in the varied conditions of test fluids, system pressure and tube size. In particular, the inside diameters of the test section tubes used in these experiments were within 9.5–57.2 mm. In some future nuclear power plants, however, the reduction of hydraulic diameter in the reactor core is planned in order to achieve higher breeding ratio of fissile materials [28–30]. Though there exist several mechanistic models to predict the deposition rate in annular flow [31–34], m_d and m_e are usually estimated from the empirically derived correlations in the film flow analysis since the deposition and entrainment of droplets are extremely complex processes. The validity of the correlations for m_d and m_e in smaller tubes should hence be investigated

Table 1
Summary of available experimental data for the deposition rate in annular flow

Reference	Fluids	D (mm)	Flow direction	Measurement technique
Cousins and Hewitt [3]	Air–water	9.5	Upward	Double film extraction
Cousins and Hewitt [3]	Air–water	31.8	Upward	Double film extraction
Govan et al. [4]	Air–water	31.8	Upward	Double film extraction
Bertodano et al. [5]	Freon 113	10.0	Upward	Double film extraction
Hewitt et al. [6]	Steam–water	12.6	Upward	Thermal method
Andreussi [7]	Air–water	24.0	Downward	Tracer method
Schadel et al. [8]	Air–water	25.4	Upward	Tracer method
Schadel et al. [8]	Air–water	42.0	Upward	Tracer method
Schadel et al. [8]	Air–water	57.2	Upward	Tracer method

Table 2
Summary of available critical heat flux data for water upward flow in round tubes with axially non-uniform heating

Reference	D (mm)	P (MPa)
Bennett et al. [10]	12.6	6.9
Lee and Obertelli [11]	9.7	3.8–11.2
Lee [12]	9.5	6.6–7.1
Lee [13]	15.9	12.4
Casterline and Matzner [14]	10.2	6.9
Biancone et al. [15]	11.6	8.4–14.2
Biancone et al. [15]	17.1	13.3–13.4
Judd et al. [16]	11.3	6.9–13.8

Table 3
Summary of experiments for the equilibrium entrainment fraction in annular flow

Reference	Fluids	D (mm)	P (MPa)	E_{eq} (%)
Cousins et al. [18]	Air–water	9.5	0.12–0.27	0–37
Cousins and Hewitt [3]	Air–water	9.5	0.14–0.28	3–38
Cousins and Hewitt [3]	Air–water	31.8	0.20–0.21	31–65
Whalley et al. [19]	Air–water	31.8	0.12–0.35	14–96
Owen et al. [20]	Air–water	31.8	0.24	17–93
Asali [21]	Air–water	22.9	0.10	0–71
Asali [21]	Air–water	42.0	0.10	0–83
Schadel et al. [8]	Air–water	25.4	0.10	15–63
Schadel et al. [8]	Air–water	42.0	0.10	10–71
Schadel et al. [8]	Air–water	57.1	0.10	10–62
Hewitt and Pulling [22]	Steam–water	9.3	0.24–0.45	1–69
Yanai [23]	Steam–water	12.0	0.34	3–69
Würtz [24]	Steam–water	10.0	3.0–9.1	12–87
Würtz [24]	Steam–water	20.0	7.1	38–92
Keeys et al. [25]	Steam–water	12.7	3.5–6.9	60–86
Nigmatulin et al. [26]	Steam–water	13.3	0.90–10	7–98
Singh et al. [27]	Steam–water	12.5	6.9	4–85
Whalley et al. [19]	Air-trichlorethane	31.8	0.27–0.28	73–98
Asali [21]	Air-glycerin	42.0	0.10	7–84

to confirm the safety of these future nuclear power plants. In view of this, the decision was made to measure the deposition rate and the entrainment fraction in the equilibrium annular flow using a small tube as the test section. In the present experiments, the test section was a round tube of 5mm in inside diameter, air and water were used as test fluids and the flow direction was vertical upward. The data were used to elucidate the applicability of available correlations for m_d and m_e to annular flow in small tubes.

2. Description of the experiments

The experiments were carried out with an adiabatic upward air–water flow loop that is shown schematically in Fig. 1. The test section was made of a stainless steel tube that was 5 mm in inside diameter. An oil-free compressor was used to supply air from the bottom of test section. Two mass flow controllers were used to measure the different ranges of air flowrate ($0–2.16 \times 10^{-3}$ kg/s; $2.16 \times 10^{-3}–12.9 \times 10^{-3}$ kg/s). Both the controllers were accurate to within ±1% of their respective full scale. A centrifugal pump derived filtrated and deionized tap water from a storage tank to air–water mixer. A cooler and a heat exchanger were used to keep the water temperature near ambient temperature. The water flowrate was measured with an oval gear flow meter that was accurate to within ±0.5%. The tube wall at the air–water mixing section was made of a porous stainless steel with 100 μm porosity to supply water as a liquid film from the periphery of the test tube. The length of porous tube was 30 mm and the inside diameter was the same as that of test section. The same porous tubes were used for the first and second liquid film extraction units that were equipped 1600 mm and 1780 mm above the mixing section, respectively.

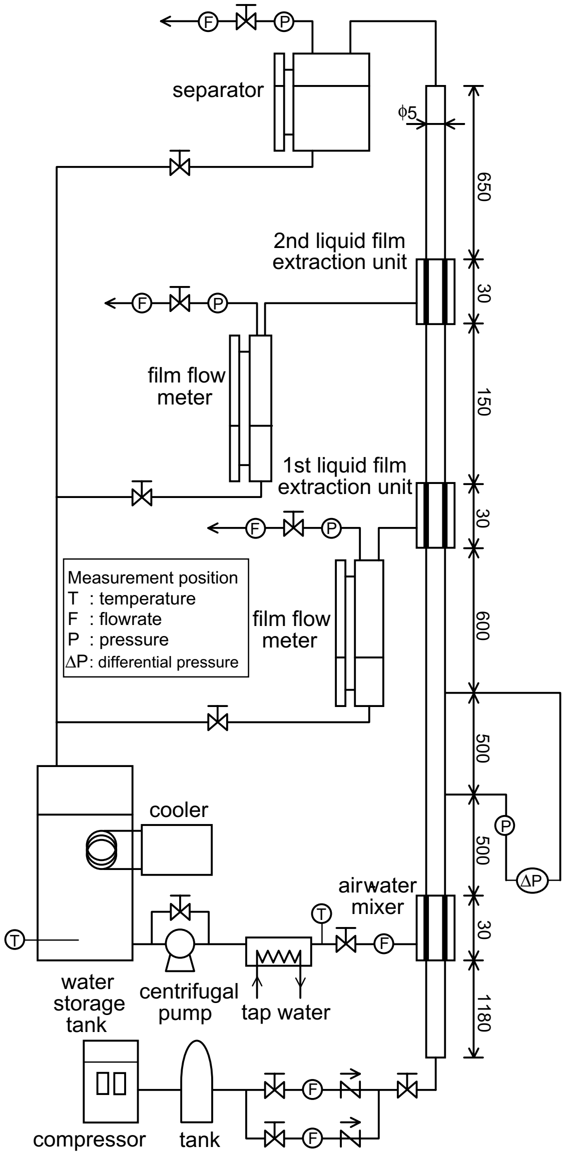

Fig. 1. Schematic diagram of experimental apparatus.

Fig. 2 shows the schematic of the flow configuration expected in the test section. The liquid film flow is established at the air–water mixer but a portion of liquid is entrained into the gas core flow as the liquid phase goes up the test tube; a portion of the entrained droplets are then deposited on the liquid film. Sufficiently downstream from the mixing section, the deposition rate might be balanced with the entrainment rate. Thus, the flowrates of droplets and liquid film become almost constant and the flow reaches quasi-equilibrium state. In the present flow loop, the distance between the air–water mixer and the first liquid film extraction unit was approximately 320 tube diameters. From an available correlation [35], 250 D is sufficient to ensure fully developed annular flow for all the experimental conditions tested. It is hence considered that the flow reached the quasi-equilibrium state at the first extraction unit. Here,

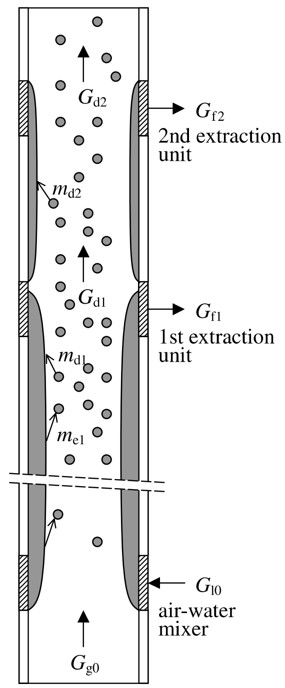

Fig. 2. Flow configuration expected in the test section.

the liquid film was completely extracted by means of the porous wall extraction technique [9]. The extracted liquid was stored in the film flowrate measuring tank to calculate the flowrate of extracted liquid from the increasing speed of water level in the tank. The increasing speed was measured with a stopwatch. The measurement error of extracted liquid flowrate is estimated less than ±2%. Since the film flowrate was unsteady, some of the gas phase should also be extracted for the complete extraction of liquid film. Two rotameters were used to measure different ranges of the extracted air flowrate (one for the range of 2.16×10^{-5}–2.16×10^{-4} kg/s with the accuracy of ±2% full scale and the other for the range of 2.16×10^{-4}–2.16×10^{-3} kg/s with the accuracy of ±5% full scale). When the extracted gas flowrate was too small, the extracted liquid flowrate increased with the extracted gas flowrate. While, when the adequate amount of air was extracted, the extracted liquid flowrate was insensitive to the extracted gas flowrate. This implies that the liquid film was completely extracted but the droplets were not readily diverted into the porous section. In the present experiments, the ratio of extracted air flowrate was varied within the range of 1–20% of total air flowrate. It was postulated that the extracted liquid flowrate corresponded to the film flowrate in the case that the variation of extracted liquid flowrates was less than 5% even when the extracted gas flowrate was doubled. As indicated in Fig. 3 with the open circles, this criterion was satisfied in most experimental conditions tested. However, as indicated in the same figure with the cross symbols, it was not satisfied in some cases. It is found in Fig. 3 that the boundary between the two groups roughly corresponds to the following correlation by Wallis for the transition to annular flow [36]

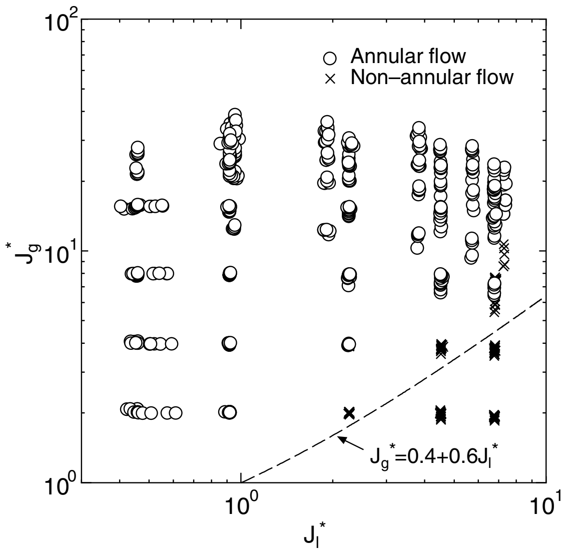

Fig. 3. Experimental conditions in which the extracted liquid flowrate became constant.

$$J_g^* = 0.4 + 0.6J_l^* \tag{4}$$

Here, the dimensionless superficial velocity is defined by

$$J_k^* = J_k\sqrt{\frac{\rho_k}{gD(\rho_l-\rho_g)}} \tag{5}$$

where g is the gravitational acceleration, ρ_l is the liquid density and the subscript k denotes g or l. It is hence confirmed that the flowrate of extracted liquid does not become constant when the flow pattern in the tube is other than annular flow. In the first series of experiments, the liquid was removed only from the first extraction unit to measure E_{eq}. The experimental data of E_{eq} measured in this study are listed in Table 4.

As schematically shown in Fig. 2, the liquid film was completely extracted at the first extraction unit but a new liquid film was built up between the first and second extraction units due to the redeposition of droplets. The film Reynolds number Re_f at the second film extraction unit was less than 310 and did not satisfy the following empirical relation for the onset of entrainment [37] in all the measurements of deposition rate

$$Re_f \geqslant \exp\left(5.8504 + 0.4249\frac{\mu_g}{\mu_l}\sqrt{\frac{\rho_l}{\rho_g}}\right) \tag{6}$$

where μ is the viscosity. Since the entrainment rate in this redeposition section might be neglected, the flowrate of new liquid film that was extracted at the second extraction unit gave the measure of deposition rate of droplets. Since the film flowrate was generally smaller at the second extraction unit than at the first, the extracted air flowrate was varied within the reduced range of 1–5% of total air flowrate for the complete extraction of liquid film. The film flowrate at the second film extraction unit was measured with the same procedure used at the first extraction unit. The distance between the first and second film extraction units was 180 mm. Consequently, the length of redeposition section z_d equals 36 D in the present experiments.

The water temperature was measured at the exit of heat exchanger (see Fig. 1) with a type-K thermocouple. The system pressure was controlled with the valve that was equipped at the top of separator. The pressure and differential pressure were measured between the mixing section and the first extraction unit. The thermocouple, pressure transducer and differential pressure transducer were accurate to within ±2.5 K, ±20 kPa and ±3 kPa, respectively. The pressure gradient was assumed constant along the test tube to estimate the pressure at the first film extraction unit. The measurements of temperature, pressure,

Table 4
Experimental data of equilibrium entrainment fraction

P (kPa)	T (C)	G_g (kg/m^{2}s)	G_l (kg/m^{2}s)	E_{eq} (%)
420	26	329	1610	41
388	26	329	1610	39
310	26	219	1630	34
475	26	439	1270	45
464	26	441	1270	45
453	26	441	1270	46
381	26	331	1270	37
368	26	329	1270	38
280	26	220	1280	30
272	27	220	1270	29
188	27	111	1270	22
180	27	112	1270	21
542	26	539	858	56
524	26	547	839	59
450	26	440	863	52
430	26	440	847	54
359	26	330	855	43
358	26	330	850	44
348	26	330	840	44
258	26	220	851	33
256	27	220	852	34
253	26	220	852	34
164	26	111	843	19
159	26	112	844	18
158	26	112	845	17
496	25	550	416	69
499	26	550	421	68
398	26	440	420	65
399	26	441	417	65
391	26	440	419	66
318	25	330	423	57
317	25	330	422	56
310	25	330	430	57
224	26	220	417	43
224	27	220	415	42
221	26	219	432	42
147	26	111	434	17
146	26	112	415	18
145	26	112	415	19
559	26	627	204	60
552	25	628	212	60
528	26	627	213	58
477	25	550	199	59
462	26	550	206	58
444	25	550	214	58
385	26	440	210	59
379	26	440	211	57
370	25	440	218	57
297	26	330	211	55
291	26	330	212	53
284	26	330	212	54
205	26	220	215	43
204	27	220	210	42
194	26	221	217	44
142	27	111	211	17
141	26	111	208	18
140	28	111	210	15

Table 4 (*continued*)

P (kPa)	T (C)	G_g (kg/m^{2}s)	G_l (kg/m^{2}s)	E_{eq} (%)
136	25	111	211	18
228	23	173	92	16
227	23	173	98	17
224	22	173	99	17
220	23	173	100	17
309	24	345	100	34
306	24	345	102	32
299	24	345	102	32
287	24	345	102	32
268	25	264	101	30
267	25	264	101	30
262	24	264	102	30
254	25	263	102	28
243	23	173	203	20
242	23	173	202	20
238	22	173	204	20
235	22	173	204	20
324	25	345	204	51
320	23	345	205	51
313	24	345	203	52
299	24	345	203	52
279	25	264	210	42
278	27	264	203	41
274	24	264	206	42
264	25	264	203	42
389	25	440	203	57
390	25	439	203	57
380	25	440	203	56
363	25	440	203	56
216	22	86	500	6
213	22	87	500	5
260	23	173	500	18
253	23	174	501	21
251	22	174	500	21
355	24	345	501	52
355	24	345	499	52
346	24	345	499	53
305	24	263	501	40
305	25	263	504	40
301	25	263	502	40
426	25	439	501	61
426	25	439	502	62
418	25	441	505	63
251	23	86	1000	9
290	23	175	1000	20
285	23	174	1000	18
413	25	344	1000	38
399	24	344	1000	39
395	24	345	1000	39
337	25	264	1000	32
335	25	263	1000	31
326	25	263	1000	32
481	26	441	997	48
473	25	441	996	48
457	26	440	994	49
257	23	87	1500	22
320	23	174	1500	27
427	25	344	1500	38

(*continued on next page*)

Table 4 (*continued*)

P (kPa)	T (C)	G_g (kg/m^{2}s)	G_l (kg/m^{2}s)	E_{eq} (%)
403	25	345	1500	37
363	26	264	1500	32
430	22	244	89	16
430	23	244	101	17
428	22	244	102	17
424	22	244	102	17
443	22	244	203	21
442	23	244	203	20
440	23	244	203	19
435	23	244	203	19
491	25	396	198	43
488	25	395	202	44
483	25	395	204	43
472	25	395	203	44
428	23	123	500	6
425	22	123	500	6
466	23	245	498	19
465	23	244	500	17
460	23	243	501	18
513	25	395	505	41
512	25	396	500	41
505	25	395	500	41
493	25	396	501	42
436	22	123	1010	10
427	23	123	1010	7
495	23	244	995	17
485	23	244	1000	16
473	23	244	999	14
536	23	396	1000	31
527	23	396	997	33
524	23	396	1000	32
501	11	244	1500	24
539	11	330	1490	30
524	11	330	1500	28
646	23	298	112	14
646	23	298	111	16
644	23	298	116	15
640	23	298	122	14
653	23	298	199	19
652	23	297	203	17
650	23	297	204	18
645	23	297	204	17
745	25	594	189	49
742	25	594	207	49
731	25	594	201	47
718	25	594	204	48
638	23	150	500	5
663	23	297	500	16
660	23	298	493	15
656	23	296	502	14
764	25	588	509	49
761	25	587	517	49
751	25	590	509	48
672	23	298	1000	17
664	23	298	1000	13

differential pressure and the flowrates of air and water at the mixing section were recorded every one second with a data acquisition system that was connected with a personal computer. The sampling periods were within 118-1131 s depending on the increasing speed of water level in the film flowrate measuring tank. The flow conditions in the test section were kept in the steady state within the sampling periods; the root mean square values of the deviation from the averages were within 1 K for water temperature, 1% for test section pressure, 1% for pressure loss, 4% for water flowrate and 1% for air flowrate.

3. Experimental results

3.1. Deposition rate

The method described by Cousins and Hewitt [3] was used to deduce the deposition mass transfer coefficient k_d from the data of the present double film extraction experiments. Postulating that the liquid film is thin and the relative velocity between the gas phase and droplets is small, the axial variation of droplet flowrate G_d between the two liquid film extraction units is expressed by

$$\frac{dG_d}{dz} = -\frac{4}{D}k_d C \cong -\frac{4}{D}k_d \frac{\rho_g G_d}{G_g} \quad (7)$$

Further assuming that k_d is constant in the redeposition section, k_d is calculated from the present experimental data through

$$k_d = \frac{G_g D}{4\rho_g z_d} \ln \frac{G_{d1}}{G_{d2}} \quad (8)$$

where G_{d1} and G_{d2} denote the droplet flowrates at the first and second film extraction units, respectively. All the experimental data of deposition rate are listed in Table 5.

Many correlations for k_d that are available in literature adopted J_g or C as a parameter of primary importance [4,7,8,38–40]. Thus, the dependences of k_d on these two parameters are tested in Fig. 4(a) and (b), respectively. The figures indicate that no notable dependence on J_g is found in the present experimental conditions while k_d monotonously decreases with the increase of C. It is hence considered that the correlation for k_d should include the influence of C. In Fig. 5(a)–(d), the present experimental data are compared with the following four correlations [7,8,39,40] that account the influence of C

$$\text{Andreussi [7]}: \quad \frac{k_d}{u^*} = \frac{0.115}{1 + 2.3C/\rho_g} \quad (9)$$

Table 5
Experimental data of deposition mass transfer coefficient

No.	P (MPa)	T (C)	G_{l0} (kg/m^{2}s)	G_{d1} (kg/m^{2}s)	G_{d2} (kg/m^{2}s)	G_{g0} (kg/m^{2}s)	G_{g1} (kg/m^{2}s)	G_{g2} (kg/m^{2}s)	J_{g1} (m/s)	C_{drp} (kg/m^3)	k_d (m/s)
1	0.460	26.9	1264	597	545	440	418	409	78.3	7.30	0.050
2	0.341	20.3	845	382	341	330	323	322	79.7	4.54	0.063
3	0.339	20.4	843	384	341	330	323	320	80.3	4.51	0.065
4	0.244	20.4	853	304	256	220	209	206	72.3	3.88	0.086
5	0.242	20.4	854	310	262	220	209	204	72.8	3.93	0.084
6	0.388	20.2	424	278	252	439	430	428	93.3	2.84	0.064
7	0.301	20.2	428	251	222	329	323	321	90.1	2.62	0.076
8	0.217	17.2	414	185	154	220	216	214	82.7	2.05	0.106
9	0.215	18.3	415	184	153	220	215	213	83.6	2.02	0.108
10	0.516	19.0	214	124	103	627	614	610	99.6	1.14	0.131
11	0.513	19.0	214	124	102	627	614	607	100.2	1.13	0.138
12	0.224	18.6	202	44	25	173	170	169	63.5	0.54	0.242
13	0.224	18.7	203	44	25	173	170	168	63.6	0.54	0.240
14	0.259	18.6	201	85	65	264	258	257	83.2	0.90	0.151
15	0.257	18.6	203	86	66	264	258	255	84.0	0.91	0.160
16	0.370	17.1	203	110	92	439	430	428	96.9	1.04	0.121
17	0.248	18.6	499	105	67	173	164	162	55.4	1.56	0.171
18	0.238	18.6	499	110	72	173	164	160	57.8	1.57	0.173
19	0.338	18.3	492	266	233	345	338	335	83.7	2.98	0.076
20	0.286	18.6	500	206	170	263	258	257	75.4	2.50	0.101
21	0.285	18.6	500	208	171	264	258	255	75.7	2.50	0.103
22	0.381	18.9	1001	400	352	345	338	337	74.4	5.05	0.066
23	0.378	18.9	1000	401	351	345	338	335	75.0	5.02	0.070
24	0.309	18.9	999	318	262	264	251	247	67.9	4.28	0.091
25	0.309	18.9	991	317	262	264	250	244	68.0	4.26	0.091
26	0.449	18.9	991	480	441	440	431	429	80.4	5.73	0.048
27	0.441	18.8	210	43	25	244	239	238	45.5	0.76	0.169
28	0.440	18.7	203	42	24	244	239	237	45.6	0.72	0.175
29	0.480	18.6	196	83	66	395	386	384	67.3	1.11	0.107
30	0.478	18.7	204	89	70	395	386	382	67.7	1.18	0.113
31	0.499	18.8	498	209	176	395	386	384	64.8	2.97	0.078
32	0.498	18.8	503	211	176	395	386	382	65.0	2.99	0.082
33	0.520	19.3	993	320	263	392	372	367	60.0	4.85	0.082
34	0.518	19.3	998	322	265	393	373	363	60.4	4.85	0.082

Schadel et al. [8]: $$k_d = \frac{0.034}{D^{0.6}} \quad \text{for } C \leqslant \frac{0.078}{D^{0.6}}$$
$$\text{and } k_d = \frac{0.021}{D^{0.6}C} \quad \text{for } C > \frac{0.078}{D^{0.6}} \tag{10}$$

Sugawara [39]: $$\frac{k_d}{J_g} = 0.009\, Re_g^{-0.2} \left(\frac{C}{\rho_g}\right)^{-0.5} Pr_g^{-0.667} \tag{11}$$

Okawa et al. [40]: $$k_d \sqrt{\frac{\rho_g D}{\sigma}} = 0.0632 \left(\frac{C}{\rho_g}\right)^{-0.5} \tag{12}$$

Note that the correlation by Andreussi [7] requires the friction velocity u^* but the frictional pressure loss along the redeposition section was not measured in the present experiments. Thus, in Fig. 5(a), u^* is assumed proportional to J_g ($u^* = 0.05 J_g$). The correlations developed by Andreussi [7] and by Sugawara [39] include both C and J_g. It is however interesting to note that the collapse of present experimental data is not improved in these correlations. The correlation by Okawa et al. [40] captures the effect of C fairly well but it generally overestimates the present experimental results. Cousins and Hewitt [3] investigated the effect of the deposition length z_d on k_d in their double film extraction experiments and found that k_d initially decreases rapidly with the increase of z_d and then approaches to a constant value for long z_d. This would be because the large droplets and/or the droplets having a large radial velocity impact the wall within a short distance. The correlation by Okawa et al. [40] was derived empirically from the experimental data for various fluids that were compiled by Govan et al. [4]. In this database, the experimental data satisfying $14 < z_d/D < 19$ were selected to eliminate the dependence of k_d on z_d. It is hence considered that the overestimation seen in Fig. 5(d) is primarily caused by the longer deposition length adopted in the present

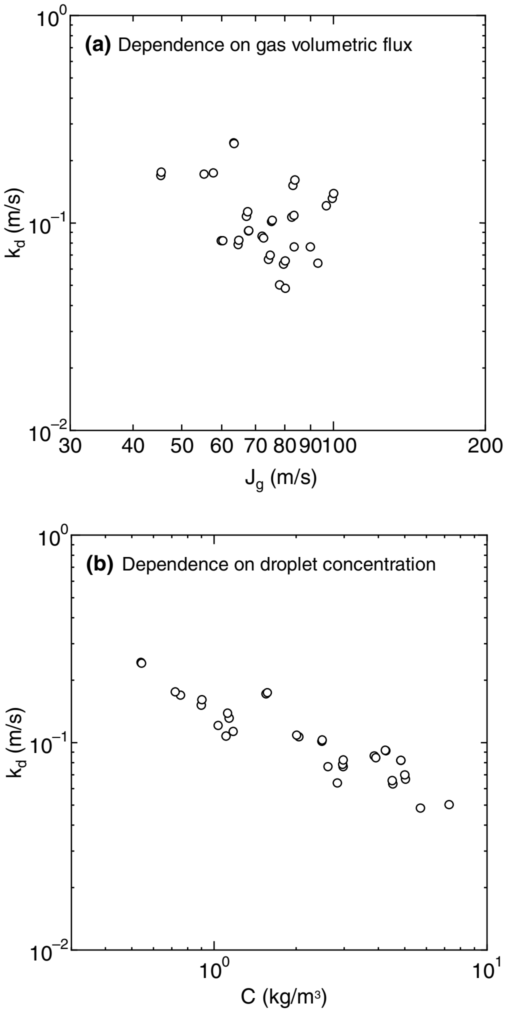

Fig. 4. Dependence of deposition mass transfer coefficient k_d on (a) gas volumetric flux J_g and (b) droplet concentration C.

experiments ($z_d/D = 36$). Therefore, the deposition mass transfer coefficient k_d that is deduced from the double film extraction experiments should include implicitly the effect of dimensionless deposition length z^* ($z^* = z_d/D$)

$$k_d = k_{d0}F(z^*) \tag{13}$$

where k_{d0} is the deposition mass transfer coefficient when z_d approaches zero and $F(z^*)$ is the correction function for z^*. As indicated with the dashed dotted line in Fig. 5(d), the present experimental data for k_d are satisfactorily correlated by

$$k_d\sqrt{\frac{\rho_g D}{\sigma}} = k_{d0}F(z^*)\sqrt{\frac{\rho_g D}{\sigma}} = 0.040\left(\frac{C}{\rho_g}\right)^{-0.5} \tag{14}$$

This result confirms that the dependence of k_d on C in the present small diameter tube is similar to that in larger tubes. It should however be noted that z_d is considered zero if the droplet entrainment coexists with the droplet deposition as in the usual situation of annular two-phase flow. The function $F(z^*)$ should therefore be determined in the future in order to use the data of double film extraction experiments for the model development studies of deposition rate.

The experimental data of k_d available in literature [3,4,8] are plotted against C in Fig. 6 to compare the present results with those for air–water annular flow in larger tubes. There exists considerable scattering since the gas density and deposition length among other parameters would also have the influence on k_d. However, the figure may indicate that the important feature of droplet deposition does not change significantly even if the tube size is reduced to 5 mm.

3.2. Entrainment rate

At the first liquid film extraction unit, annular flow might reach the equilibrium state. Thus, the following relation is assumed at the first unit:

$$m_{e1} \cong m_{d1} \cong k_{d0}C_1 = \frac{k_d C_1}{F(z^*)} \tag{15}$$

where m_{e1}, m_{d1} and C_1 are the entrainment rate, deposition rate and droplet concentration at the first film extraction unit, respectively; k_d is the deposition mass transfer coefficient calculated from the data of present double film extraction experiments through Eq. (8). To correlate E_{eq} measured in varied experimental conditions, Okawa et al. [40] assumed that m_e is expressed in terms of the following dimensionless number π_e, that denotes the ratio of interfacial shear force to surface tension force acting on the surface of liquid film

$$\pi_e = \frac{f_i \rho_g J_g^2 \delta}{\sigma} \tag{16}$$

where f_i is the interfacial friction factor, δ is the film thickness and σ is the surface tension. The values of $k_d C_1/\rho_l$ measured in the present double film extraction experiments are plotted against π_e in Fig. 7(a). In the calculation of δ that is included in π_e, f_i is evaluated from the correlation by Wallis [36]

$$f_i \rho_g J_g^2 \cong f_w \rho_l u_f^2 \cong f_w \rho_l \left(\frac{D}{4\delta} J_f\right)^2 \tag{17}$$

$$f_i = 0.005\left(1 + 300\frac{\delta}{D}\right) \tag{18}$$

$$f_w = 0.005 \tag{19}$$

where f_w is the wall friction factor. Note that Eq. (17) expresses the force balance between the interfacial

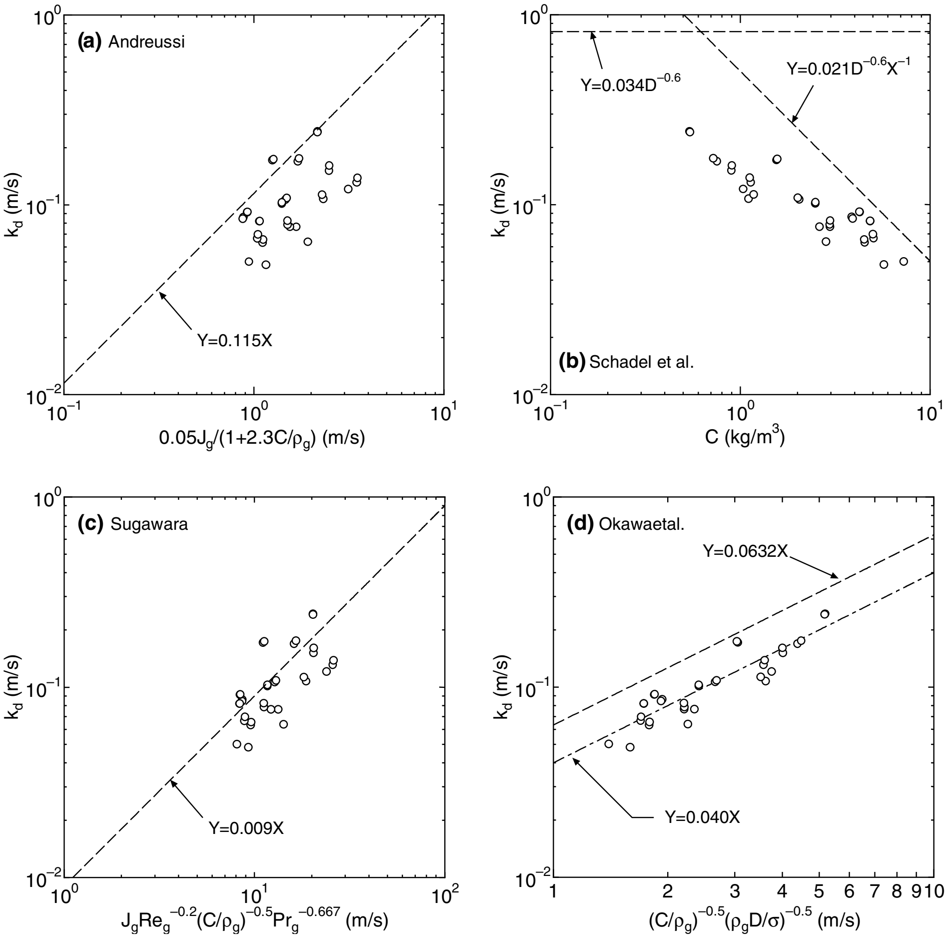

Fig. 5. Comparison of experimental data of deposition mass transfer coefficient k_d with the correlations by (a) Andreussi [7], (b) Schadel et al. [8], (c) Sugawara [39], and (d) Okawa et al. [40].

shear force and wall friction force acting on the liquid film. In Fig. 7(b)–(d), the same experimental data are plotted against the three dimensionless groups that are used in the following correlations by Govan et al. [4], Kataoka et al. [41] and Lopez de Bertodano et al. [5]:

$$\frac{m_e}{G_g} = 5.75 \times 10^{-5} \pi_{gov}^{0.316}; \quad \pi_{gov} = \left(G_f - \frac{Re_{fc}\mu_l}{D} \right)^2 \frac{D\rho_l}{\sigma \rho_g^2} \tag{20}$$

$$\frac{m_e D}{\mu_l} = 6.6 \times 10^{-7} \pi_{kat};$$

$$\pi_{kat} = Re_l^{0.74} Re_f^{0.185} \left[We_g \left(\frac{\rho_l - \rho_g}{\rho_g} \right)^{1/3} \right]^{0.925} \left(\frac{\mu_g}{\mu_l} \right)^{0.26} \tag{21}$$

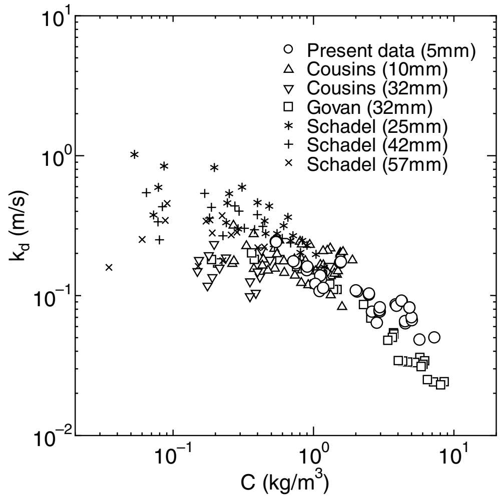

Fig. 6. Comparisons of present experimental data of deposition mass transfer coefficient with those for air–water annular flow in larger tubes.

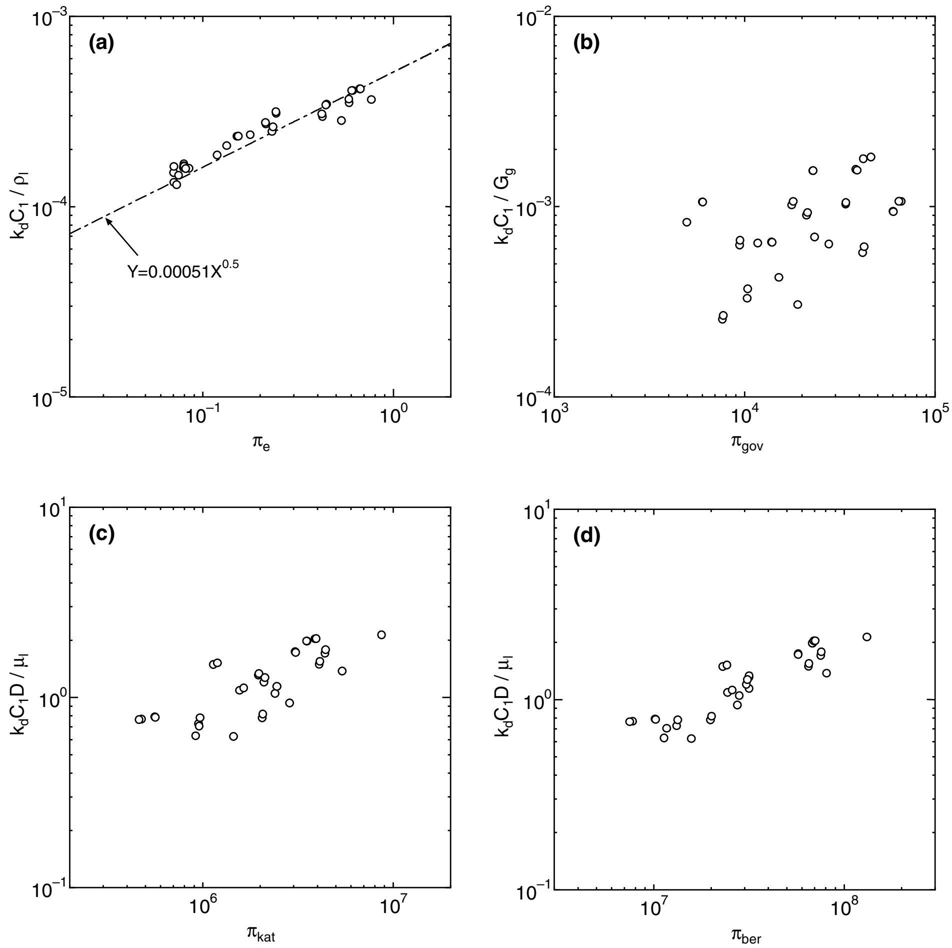

Fig. 7. Dependence of measured entrainment rate on the dimensionless groups proposed by (a) Okawa et al. [40], (b) Govan et al. [4], (c) Kataoka et al. [41], and (d) Lopez de Bertodano et al. [5].

$$\frac{m_e D}{\mu_l} = 0.5 \times 10^{-7}\pi_{ber};$$

$$\pi_{ber} = (Re_f - Re_{fc})We_g\left(\frac{\rho_l}{\rho_g}\right)^{1/2} \tag{22}$$

where the gas phase Weber number We_g is defined by

$$We_g = \frac{\rho_g J_g^2 D}{\sigma} \tag{23}$$

The critical film Reynolds number for the onset of entrainment Re_{fc} is calculated by Eq. (6) in Eq. (20) while assumed equal to 80 in Eq. (22). Fig. 7(a)–(d) show that a simple dimensionless number π_e is appropriate to collapse the present experimental data of $k_d C_1$. Consequently, as indicated with the dashed dotted line in Fig. 7(a), m_{e1} may be expressed in the following functional form:

$$\frac{k_d C_1}{\rho_l} = \frac{k_{d0} F(z^*) C_1}{\rho_l} = \frac{m_{e1} F(z^*)}{\rho_l} = k_e \pi_e^n \tag{24}$$

Here, the proportionality factor k_e has the dimension of ms^{-1}. As described in the introduction, it is also possible to derive m_{e1} from the experimental data of E_{eq} if valid correlation for k_d is available. From Eqs. (2) and (24), m_{e1} is expressed in terms of E_{eq} by

$$\frac{m_{e1} F(z^*)}{\rho_l} = \frac{k_d E_{eq} J_l}{J_g} \tag{25}$$

Evaluating k_d by Eq. (14), the values of right-hand-side of Eq. (25) are plotted against π_e in Fig. 8. In the present experiments, G_{f1} was subtracted from G_{l0} to derive E_{eq} ($E_{eq} = (G_{l0} - G_{f1})/G_{l0}$). Thus, the experimental data in which $G_{f1} > 0.9G_{l0}$ were excluded to reduce the scattering due to the measurement error. Comparison of Fig. 8 with Fig. 7(a) confirms that the experimental data of E_{eq} are correlated well with the same equation of π_e, that

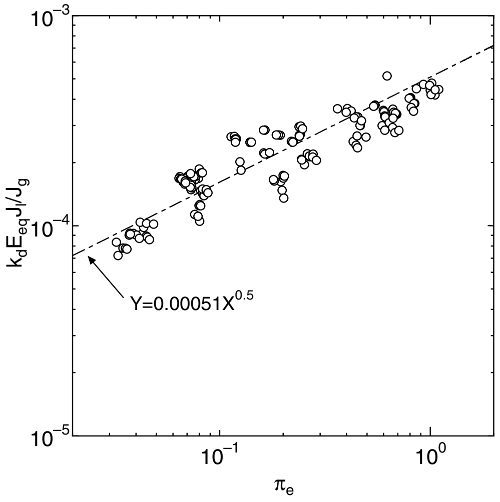

Fig. 8. Dependence of measured entrainment fraction on π_e.

was originally derived from the experimental data of deposition rate in the equilibrium state.

Ishii and Mishima [35] developed the following simple correlation for E_{eq}:

$$E_{eq} = \tanh(7.25 \times 10^{-7}\eta) \tag{26}$$

$$\eta = \left\{ We_g \left(\frac{\rho_l - \rho_g}{\rho_g} \right)^{1/3} \right\}^{1.25} Re_l^{0.25} \tag{27}$$

To compare the present results for a small tube with available ones [3,8,18–21], the experimental data of E_{eq} are plotted against η in Fig. 9. One finds that a simple dimensionless parameter η may not be sufficient to collapse these data but the present data appear not to differ significantly from other data for air–water annular flow in larger tubes.

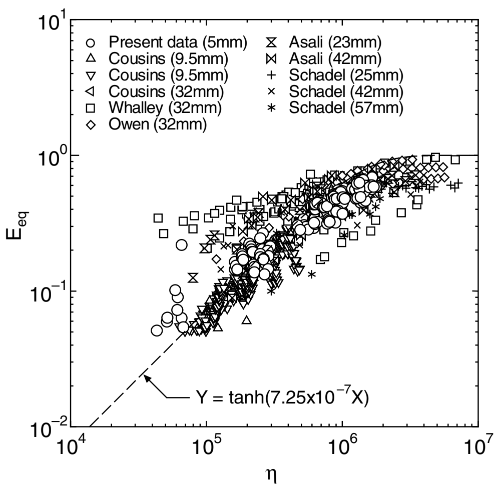

Fig. 9. Comparisons of present experimental data of equilibrium entrainment fraction with those for air–water annular flow in larger tube.

4. Conclusions

This paper provided the experimental data of the deposition rate and entrainment fraction in quasi-equilibrium annular flow. The inside diameter of the test section tube was 5mm and might be smallest in the similar experiments that were reported previously in the open literature. The present data were hence expected useful to investigate the onset of critical heat flux condition in the future nuclear power plants in which the reduction of cross-sectional area of flow channel was planned.

For the future model development studies, the dimensionless groups that were appropriate to characterize the deposition rate and entrainment rate were investigated. It was shown in the present experimental ranges that:

(1) The deposition mass transfer coefficient tended to decrease with the increase of droplet concentration in the gas core while no notable dependence on the gas flowrate was found. The dependence of the dimensionless deposition mass transfer coefficient $k_d(\rho_g D/\sigma)^{0.5}$ on the dimensionless droplet concentration (C/ρ_g) was similar to that proposed in available correlations for larger diameter tubes.
(2) The measured deposition mass transfer coefficients were generally smaller than those predicted by available correlations. The rather long deposition length adopted in the present experiments was considered the primary cause of this discrepancy. This suggested that the effect of deposition length should be corrected to derive a reliable correlation for the deposition mass transfer coefficient from the data of double film extraction experiments.
(3) The ratio of interfacial shear force to surface tension force acting on the surface of liquid film collapsed well the experimental data for the entrainment rate of droplets and was expected an appropriate dimensionless number for the correlation of entrainment rate. This result was also consistent with available knowledge of the droplet entrainment for larger diameter tubes.

Acknowledgment

This work was funded by the Institute of Applied Energy (IAE), and Ministry of Economy, Trade and Industry (METI).

References

[1] G.F. Hewitt, Burnout, in: G. Hetsroni (Ed.), Handbook of Multiphase Systems, McGraw-Hill, New York, 1982 (Section 6.4).

[2] P.B. Whalley, Boiling, Condensation and Gas–Liquid Flow, Oxford Science Publications, Oxford, 1987 (Chapter 19).

[3] L.B. Cousins, G.F. Hewitt, Liquid phase mass transfer in annular two-phase flow: droplet deposition and liquid entrainment, AERE-R5657, 1968.

[4] A.H. Govan, G.F. Hewitt, D.G. Owen, T.R. Bott, An improved CHF modelling code, in: Proceedings of 2nd UK National Heat Transfer Conference, 1988, pp. 33–48.

[5] M.A. Lopez de Bertodano, A. Assad, S.G. Beus, Experiments for entrainment rate of droplets in the annular regime, Int. J. Multiphase Flow 27 (2001) 685–699.

[6] G.F. Hewitt, H.A. Kearsey, R.K.F. Keeys, Determination of rate of deposition of droplets in a heated tube with steam–water flow at 1000 psia, AERE-R6118, 1969.

[7] P. Andreussi, Droplet transfer in two-phase annular flow, Int. J. Multiphase Flow 9 (6) (1983) 697–713.

[8] S.A. Schadel, G.W. Leman, J.L. Binder, T.J. Hanratty, Rates of atomization and deposition in vertical annular flow, Int. J. Multiphase Flow 16 (3) (1990) 363–374.

[9] G.F. Hewitt, Liquid-phase mass transfer rate in annular flow, in: G. Hetsroni (Ed.), Handbook of Multiphase Systems, McGraw-Hill, New York, 1982 (Section 10.2.2.4).

[10] A.W. Bennett, G.F. Hewitt, H.A. Kearsey, R.F.K. Keeys, D.J. Pulling, Studies of burnout in boiling heat transfer to water in round tubes with non-uniform heating, AERE-R5076, 1966.

[11] D.H. Lee, J.D. Obertelli, An experimental investigation of forced convection burnout in high pressure water, Part 2. Preliminary results for round tubes with non-uniform axial heat flux distribution, AEEW-R309, 1963.

[12] D.H. Lee, An experimental investigation of forced convection burnout in high pressure water, Part 3. Long tubes with uniform and non-uniform axial heating, AEEW-R355, 1965.

[13] D.H. Lee, An experimental investigation of forced convection burnout in high pressure water, Part 4. Large diameter tubes at about 1600 psi, AEEW-R479, 1966.

[14] J.E. Casterline, B. Matzner, Burnout in long vertical tubes with uniform and cosine heating using water at 1000 psia, Columbia University, TID-21031, 1964.

[15] F. Biancone, A. Campanile, G. Galimi, M. Goffi, Forced convection burnout and hydrodynamic instability experiments for water at high pressure, Part 1. Presentation of data for round tubes with uniform and non-uniform power distribution, EUR2490e, 1965.

[16] D.F. Judd, R.H. Wilson, C.P. Welch, R.A. Lee, J.W. Ackerman, Non-uniform heat generation experimental program, Quarterly progress report no. 7, BAW-3238-7, 1965.

[17] P.B. Whalley, G.F. Hewitt, The correlation of liquid entrainment fraction and entrainment rate in annular two-phase flow, AERE-R9187, 1978.

[18] L.B. Cousins, W.H. Denton, G.F. Hewitt, Liquid mass transfer in annular two-phase flow, in: Proceedings of Symposium on Two-Phase Flow, Exeter, 1965, Paper C4.

[19] P.B. Whalley, G.F. Hewitt and P. Hutchinson, Experimental wave and entrainment measurements in vertical annular two-phase flow, AERE-R7521, 1973.

[20] D.G. Owen, G.F. Hewitt, T.R. Bott, Equilibrium annular flows at high mass fluxes; data and interpretation, PCH Physicochem. Hydrodyn. 6 (1985) 115–131.

[21] J.C. Asali, Entrainment in vertical gas–liquid annular flows, Ph.D. thesis, University of Illinois, 1983.

[22] G.F. Hewitt, D.J. Pulling, Liquid entrainment in adiabatic steam–water flow, AERE-R5374, 1969.

[23] M. Yanai, Study on boiling heat transfer in a flow channel, Ph.D. Thesis, Kyoto University, 1971. (in Japanese).

[24] J. Würtz, An experimental and theoretical investigation of annular steam–water flow in tube and annuli at 30 to 90 bar, Riso Report No. 372, 1978.

[25] R.F.K. Keeys, J.C. Ralph, D.N. Roberts, Liquid entrainment in adiabatic steam–water flow at 500 and 1000 psia, AERE-R6293, 1970.

[26] B.I. Nigmatulin, V.I. Malyshenko, Y.Z. Shugaev, Investigation of liquid distribution between the core and the film in annular dispersed flow of steam/water mixture, Teploenergetika 23 (1976) 66–68.

[27] K. Singh, C.C. St. Pierre, W.A. Cargo, E.O. Moeck, Liquid film flowrates in two-phase flow of steam and water at 1000 psia, AIChE J. 15 (1969) 51–56.

[28] Y. Sakashita, T. Yokoyama, Y. Tsuboi, Core characteristics of breeding BWR for BARS (BWR with advanced recycle system), in: Proceedings of 7th International Conference on Nuclear Engineering, 1999, Paper no. 7328.

[29] T. Okubo, T. Shirakawa, R. Takeda, T. Yokoyama, T. Iwamura, S. Wada, Conceptual designing of reduced-moderation water reactors (1) design for BWR type reactors, in: Proceedings of 8th International Conference on Nuclear Engineering, 2000, Paper no. 8422.

[30] K. Hibi, T. Kugo, H. Tochihara, S. Shimada, T. Okubo, T. Iwamura, S. Wada, Conceptual designing of reduced-moderation water reactors (2) design for PWR type reactors, in: Proceedings of 8th International Conference on Nuclear Engineering, 2000, Paper no. 8423.

[31] P.W. James, G.F. Hewitt, P.B. Whalley, Droplet motion if two-phase flow, AERE-R9711, 1980.

[32] P. Andreussi, B.J. Azzopardi, Droplet deposition and interchange in annular two-phase flow, Int. J. Multiphase Flow 9 (1983) 681–695.

[33] K.J. Hay, Z.-C. Liu, T.J. Hanratty, Relation of deposition to drop size when the rate law is nonlinear, Int. J. Multiphase Flow 22 (1996) 829–848.

[34] E.A. Matida, K. Nishino, K. Torii, Statistical simulation of particle deposition on the wall from turbulent dispersed pipe flow, Int. J. Fluid Flow 21 (2000) 389–402.

[35] M. Ishii, K. Mishima, Droplet entrainment correlation in annular two-phase flow, Int. J. Heat Mass Transfer 32 (1989) 1835–1846.

[36] G.B. Wallis, One-Dimensional Two-Phase Flow, McGraw-Hill, New York, 1969 (Chapter 11).

[37] D.G. Owen, G.F. Hewitt, A proposed entrainment correlation, AERE-R12279, 1986.

[38] T. Saito, E.D. Hughes, M.W. Carbon, Multi-fluid modeling of annular two-phase flow, Nucl. Eng. Des. 50 (1978) 225–271.

[39] S. Sugawara, Droplet deposition and entrainment modeling based on the three-fluid model, Nucl. Eng. Des. 122 (1990) 67–84.
[40] T. Okawa, T. Kitahara, K. Yoshida, T. Matsumoto, I. Kataoka, New entrainment rate correlation in annular two-phase flow applicable to wide range of flow condition, Int. J. Heat Mass Transfer 45 (2002) 87–98.
[41] I. Kataoka, M. Ishii, A. Nakayama, Entrainment and deposition rates of droplets in annular two-phase flow, Int. J. Heat Mass Transfer 43 (2000) 1573–1589.